2018 IEEE Intelligent Vehicles Symposium (IV)
Changshu, Suzhou, China, June 26-30, 2018

Generalized B-spline Camera Model

Johannes Beck[1], Christoph Stiller[1]

Abstract— **Previously proposed camera calibration methods either use a local camera model in a complex, cumbersome, time consuming and often manual calibration process or a lens specific global camera model, which can be automatically calibrated by simply recording images of chessboards. The drawback of using a global hand crafted camera model is its limited capability of modeling distortions caused by the mounted lens or optical devices in front of the lens like windshields.**

Therefore, we propose a local camera model based on B-splines which can handle various distortions. Moreover, it will be shown how such a model can be calibrated in an easy-to-use calibration process which were up to now only applicable to global camera models.

We demonstrate the benefit of using the proposed local camera model by an extensive evaluation using single and multi-camera setups with different types of lenses, some mounted behind a windshield.

I. INTRODUCTION

To get automated driving into the market, it should work reliably in as many scenarios as possible: on highways and cities, during rain and direct sun. It should also be robust toward sensor failures. Beside other sensors, cameras play an important role as they are cheap and provide rich information about the environment. Since a single camera has a limited field of view and is not safe from sensor failures, multi-camera solutions are used in practice. Usually some forward-facing cameras are mounted behind the windshield whereby side-facing wide angle cameras can be used for blind spot detection and rear-facing cameras for parking.

In order to safely navigate a car in various environments a high-level understanding of the surrounding is required: where is the ego lane located, are there any cars in front blocking the road, is there a pedestrian crossing the street, what is the state of the traffic light? To gain such a high-level understanding of the scene, low-level and high-level machine vision algorithms like visual odometry, sematic labeling, object detection, self-localization, and many more are used and fused together. Knowing the pose of the cameras in the vehicle (extrinsic camera calibration) and the mapping between the 3D world and the camera image plane (intrinsic camera calibration) makes it possible to efficiently implement such tasks.

In the past, many approaches for intrinsic and extrinsic camera calibration were proposed. They can be mainly divided into two different groups depending on how the camera model is mathematically described. On the one hand discrete camera models are defined by a discrete mapping between image pixels and viewing rays. The calibration process of such a system is complex as lots of measurements are needed to estimate the huge number of parameters. This is usually achieved by using an active target and multiple shots per position. Thus, global camera models are commonly used in practice, as they can be integrated in a simple calibration process. On the other hand global camera models are hand crafted for special types of lenses like pinhole, fisheye or catadioptric lenses. To cope with imperfections during manufacturing and lens misplacement, non-linear distortion terms are added to the camera model. However, global camera models might fit for certain lenses, but depending on the type of distortion resulting from the lens and optical devices in front of the camera (e.g. windshields), the modelling error can be significant.

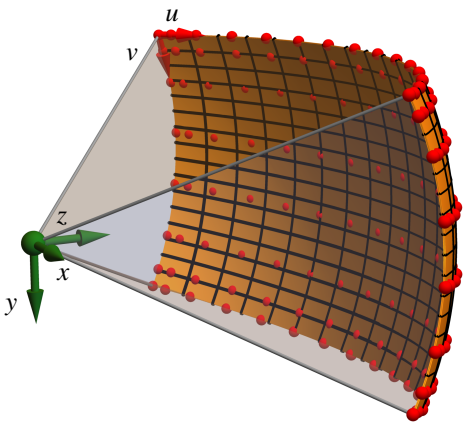

Fig. 1: B-spline camera model. The single viewpoint camera model is described by a clamped B-spline from image space (u,v) to viewing rays in (x,y,z). The viewing ray for a pixel at (u,v) is defined by the optical center shown in green and the B-spline point on the yellow surface. The red spheres are the control points of the B-spline.

In this paper, we present a generalized local camera model based on B-splines. Due to the local formulation it can cope with almost arbitrary distortions and the smoothness and fidelity can be easily adjusted. This makes it suitable for many lenses and all kinds of smooth distortions. In addition, the calibration process is as simple as for global camera models. Flat chessboard patterns are used as calibration targets and the calibration problem is formulated as a joint optimization of the poses and the camera model using a novel residual term. This makes it suitable for multi-camera setups

[1]The authors are with Institute of Measurement and Control Systems, Karlsruhe Institute of Technology (KIT), 76131 Karlsruhe, Germany {johannes.beck, stiller}@kit.edu

with non-overlapping field of views.

After discussing related work in Section II, we present our generalized local camera model in Section III. By comparing that model with a global camera model in Section IV, we show that our camera model accurately describes non-isotropic projections such as cameras mounted behind a windshield. In Section V we finally summarize in the generalized camera model and give future research directions.

II. RELATED WORK

Camera models are defined by either a discrete / local or a global mapping. A discrete camera model defines the mapping between image pixels and viewing rays only at discrete points. Usually there are no assumptions between neighboring pixels which make it suitable for any kind of distortions. In [1], the pixels are replaced by a ray pixel or a *raxel*. A *raxel* covers both the geometry of a viewing ray and radiometric properties like brightness and wavelength response. For calibration two active targets (displays) with a known distance to each other and an image device mounted on a rotary platform are used. This approach is further developed in [2] to reduce the calibration complexity by estimating the poses of the active target at the expense of having at least three measurements per ray. It is also shown how the full field of view can be calibrated. As having only a discrete camera model makes it hard for further tasks like rectification or structure from motion in [3] a smooth camera model is proposed by using radial basis functions.

Discrete camera models have a huge number of parameters because one ray per pixel is estimated. In contrast, global camera models are fully defined by only a small set of parameters. There are several types like pinhole camera model with distortions ([4], [5]) or omnidirectional camera models ([6]), only to name a few. A good overview of radial symmetric camera models can be found in [7].

Global camera models are widely used due to a simple calibration process, as only recorded images of flat targets are needed. In contrast, discrete camera models can handle arbitrary distortions (see [8]), but due to the high number of parameters no simply calibration process can be used.

There is recent work on how a local camera model can be calibrated using flat chessboards. Rosebrock et. al. ([9], [10]) proposed a B-Spline non-single viewpoint camera model using Plücker coordinates [11]. The main difference to the work presented here is the estimation process. They use a multi-step approach by first using linear calibration [12] to estimate viewing rays of a small region of the image and then subsequently add more chessboard images with sufficient overlap with the already calibrated area. A bundle adjustment problem is solved by estimating discrete rays and the chessboard poses. The final step is fitting a B-spline camera model to the estimated discrete rays. This entire process is hard to get done without manual intervention and cannot be easily extended to multi-camera setups with non-overlapping field of views, as no full bundle adjustment problem with all intrinsic and extrinsic camera parameters are formulated and solved.

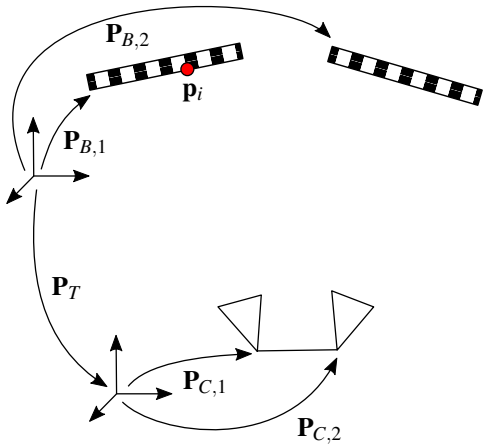

Fig. 2: The calibration setup. We use full bundle adjustment and optimize one pose per camera $\mathbf{P}_{C,i}$, one pose per board $\mathbf{P}_{B,j}$, a time dependent pose for each captured image $\mathbf{P}_{T,k}$ and the intrinsic camera parameters jointly. The residual terms are based on the chessboard corner position $\mathbf{p}_i$ and the observed corner in the image plane $\mathbf{m}_i$ (not shown).

III. GENERALIZED LOCAL CAMERA MODEL

A camera model is fully defined by either using a forward or backward model [7]. The forward model is defined as $\mathcal{P}_F : \mathbb{R}^3 \to \mathbb{R}^2$, which projects a 3D point in space to the two-dimensional image space. The backward model is defined as $\mathcal{P}_B : \mathbb{R}^2 \to \mathbb{P}^3$, which maps a two-dimensional image point to a line in $\mathbb{R}^3$, which is called viewing ray. Here, as we consider only single viewpoint camera models, all viewing rays cross at a single point and the degrees of freedom of a viewing ray is two (a unit vector).

A. Formulation

We directly model the backward projection function by a B-spline as in [10]. A one-dimensional B-Spline $\mathbf{f} : \mathbb{R} \to \mathbb{R}$ is defined as ([13])

$$f(x) = \sum_i a_i B_{i,k,\mathbf{t}}(x)\,, \tag{1}$$

where k is the spline order, $\mathbf{t}$ the non-decreasing knot sequence, $a_i \in \mathbb{R}$ the control points and B the basis. The basis is defined as

$$B_{i,0,\mathbf{t}}(x) = \begin{cases} 1 & \text{if} \quad t_i \le x < t_{i+1} \\ 0 & \text{otherwise} \end{cases} \tag{2}$$

$$B_{i,n,\mathbf{t}}(x) = \frac{x - t_i}{t_{i+n} - t_i} B_{i,n-1}(x) + \frac{t_{i+n+1} - x}{t_{i+n+1} - t_{i+1}} B_{i+1,n-1}(x)\,. \tag{3}$$

The B-spline is used to model the backward projection as $\mathbf{f}_C : \mathbb{R}^2 \to \mathbb{R}^3$, which yields to

$$\mathbf{f}_C(u,v) = \sum_i \sum_j \mathbf{a}_{i,j} B_{i,k,\mathbf{t}}(u) B_{j,k,\mathbf{t}}(v) \tag{4}$$

$$\mathcal{P}_B(u,v) = \frac{\mathbf{f}_C(u,v)}{\|\mathbf{f}_C(u,v)\|}\,, \tag{5}$$

where u and v are the image coordinates and the control points $\mathbf{a}_{i,j} \in \mathbb{R}^3$ are the intrinsic parameters (see Fig. 1). The

output is a three-dimensional vector, describing the direction of the viewing rays.

B. Parameter Estimation

For calibration the same setup as described in [14] is used. A non-linear least squares problem is solved by optimizing one pose per chessboard $\mathbf{P}_B$, one pose per camera $\mathbf{P}_C$ and a time dependent pose for each captured image $\mathbf{P}_T$ (see Fig. 2). Associated chessboard corners in image space $\mathbf{m}_i$ and the known chessboard corner position $\mathbf{p}_{B,i}$ are used as measurements. For global camera models the reprojection error is usually minimized:

$$\mathbf{p}_{C,i} = \mathbf{P}_C \mathbf{P}_T \mathbf{P}_B^{-1} \mathbf{p}_{B,i} \tag{6}$$

$$\mathbf{e}_{r,i} = \mathbf{m}_i - \mathcal{P}_F(\mathbf{p}_{C,i}) \tag{7}$$

This means that the chessboard corner positions $\mathbf{p}_{B,i}$ are at first transformed into the camera coordinate system ($\mathbf{p}_{C,i}$) and then projected onto the image plane using the camera model. The reprojection error is the distance between the projected position from the detected corner pixel position and the detected chessboard image position $\mathbf{m}_i$. If one assumes that the measurements $\mathbf{m}$ are Gaussian distributed, a maximum likelihood estimator can be formulated as a non-linear least squares problem.

As the camera model is formulated as a backward model, the generally used projection error is not feasibly because in general the B-spline cannot be easily inverted. In order to estimate the B-spline efficiently, a residual in the camera coordinate system is required. One could use the angle

$$\alpha = \arccos\left(\frac{\mathbf{p}_{C,i}}{\|\mathbf{p}_{C,i}\|} \cdot \mathcal{P}_B(\mathbf{m}_i)\right) \tag{8}$$

between the direction of the viewing ray and the direction vector resulting from the camera model at the detected corner pixel position in image space $\mathbf{m}_i$ (see Fig. 3).

This residual can cause problems in a non-linear least squares formulation, as the $\arccos(x)$ function is non-continuous and the derivative has a singularity at $x = -1$ and $x = 1$.

Eq. 8 is approximated by using the cord length d_c instead of the angle, which can be calculated as (see Fig. 3 and [15])

$$d_c = \|\mathbf{e}_{c,i}\| \tag{9}$$

$$\mathbf{e}_{c,i} = \frac{\mathbf{p}_{C,i}}{\|\mathbf{p}_{C,i}\|} - \mathcal{P}_B(\mathbf{m}_i)\,. \tag{10}$$

This residual can be easily integrated in a non-linear least squares formulation. Furthermore, another approximation especially for the B-spline camera model is made. During estimation the normalization of the viewing ray is omitted, which yields to (see Fig. 3):

$$d_f = \left\|\mathbf{e}_{f,i}\right\| \tag{11}$$

$$\mathbf{e}_{f,i} = \frac{\mathbf{p}_{C,i}}{\|\mathbf{p}_{C,i}\|} - \mathbf{f}_C(\mathbf{m}_i) \tag{12}$$

This residual term d_f is faster to compute and more stable as it does not have singularities. Also the Jacobian evaluation is simpler and faster.

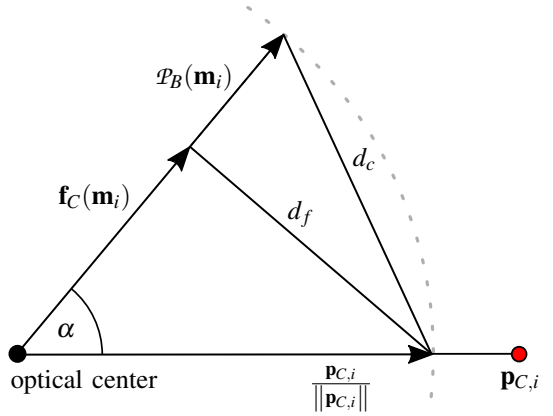

Fig. 3: Chessboard corner residuals using a forward projection camera model. Shown are three different residuals: The angle α between the viewing ray of the camera model $\mathcal{P}_B(\mathbf{m}_i)$ and the observed direction of the observation $\mathbf{p}_{C,i}$, the cord length d_c and the distance d_f between the non-normalized B-spline viewing ray $\mathbf{f}_C(\mathbf{m}_i)$ and $\mathbf{p}_{C,i}/\|\mathbf{p}_{C,i}\|$.

As the pixel position of the chessboard corners $\mathbf{m}$ are measurements and not parameters of the non-linear least squares problem and the B-spline basis does only depend on that position, the basis can be evaluated beforehand:

$$b_{\mathbf{m}_i,p,q} = B_{p,k,\mathbf{t}}(m_{1,i}) B_{q,k,\mathbf{t}}(m_{2,i}) \tag{13}$$

So to summarize the optimal poses $\mathbf{P}_B$, $\mathbf{P}_T$, $\mathbf{P}_C$ and intrinsics $\mathbf{a}$ are estimated by

$$\underset{\mathbf{P}_B,\mathbf{P}_T,\mathbf{P}_C,\mathbf{a}}{\arg\min} \frac{1}{2} \sum_i \left\|\mathbf{e}_{f,i}\right\|^2, \tag{14}$$

where

$$\mathbf{e}_{f,i} = \frac{\mathbf{p}_{C,i}}{\|\mathbf{p}_{C,i}\|} - \sum_j \sum_k \mathbf{a}_{j,k} b_{\mathbf{m}_i,j,k} \tag{15}$$

and $\mathbf{p}_{C,i}$ is as in Eq. 6.

To be able to estimate only one pose per chessboard, the detected chessboard corners need to be globally associated. We use codes around the chessboards as seen in Fig. 4. The code carries information about a unique identifier of the chessboard and the origin of coordinate system of the corner indices. For details see [14].

IV. EVALUATION

In this section, the proposed B-spline camera model is compared with a global one. First, the chosen parameters of the B-spline camera model are discussed and a single camera setup with a pinhole and fisheye lens is presented. After that, the influence of having a windshield in front of the camera is studied and a surround view setup with six cameras is calibrated. A summary of the results of the three different calibration setups are given in Tab. I.

A. B-spline parameters

The parameters of the B-spline camera model are the number of control points $\mathbf{a}$, the order k and the knot vector $\mathbf{t}$. The knot vector is chosen in such a way that the control

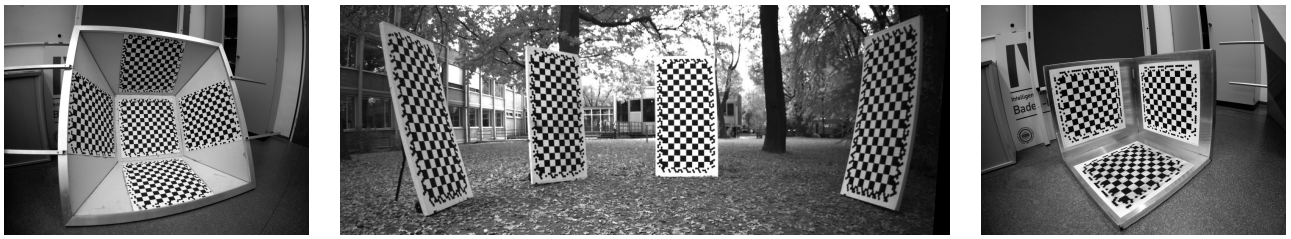

Fig. 4: The chessboards patterns. For calibration the frustum (left) and flat boards (middle), for evaluation the cube (right) are used.

Camera setup	Focal length in mm	Processing time in s (global / B-spline)	#corners (#imgs)		Reprojection error in px (calibration / evaluation)	
			Calibration	Evaluation	Global camera model	B-spline camera model
Single pinhole camera	4	100 / 142	120925 (337)	68624 (320)	0.156 / 0.157	0.140 / 0.152
Single fisheye camera	2	128 / 281	192429 (356)	70532 (319)	0.163 / 0.180	0.156 / 0.204
Windshield perpendicular	4	472 / 798	90139 (738)	32508 (381)	0.318 / 0.262	0.273 / 0.257
Windshield horizontal	4	371 / 607	72514 (465)	22766 (284)	0.525 / 0.520	0.195 / 0.223
Camera front 1	5	626 / 734	46103 (392)	-	0.441 / -	0.395 / -
Camera front 2	5		45289 (392)	-	0.441 / -	0.356 / -
Camera front 3	5		47252 (392)	-	0.451 / -	0.360 / -
Camera left	4		32720 (392)	-	0.360 / -	0.297 / -
Camera right	4		37248 (392)	-	0.331 / -	0.269 / -
Camera rear	1.3		22816 (392)	-	2.140 / -	0.271 / -

TABLE I: Summary of the results of the different calibration setups used for comparing a global camera model with our B-spline camera model.

points are evenly distributed in u and v and that the function hits the control points at the edge of the image. The order k influences the smoothness, as the B-spline is C^{k-1} continuous. The higher the number k the smoother the function, but the more non-zero elements the basis B has (see Eq. 3). This yields to a denser problem and significantly increases the estimation time. As a non-linear least squares solver is used, first and second derivatives of the B-spline are calculated. We chose $k = 4$ to get a C^1 continuous second derivative. The control points are laid out as a grid in image space. We chose one control point per 100px, which showed a good balance between the number of parameters, the computation time and the modelling error for various lenses.

B. Single camera calibration

For the single camera evaluation a 2.8MP gray scale CCD camera is used (Flir Flea3 FL3-GE-28S4M-C). For each lens two sequences with different calibration patterns are recorded, one for calibration and one for testing. For calibration, the frustum (see Fig. 4 left) is used and a joint optimization of the intrinsic camera model parameters and the poses (see Fig. 2) are performed. To compare calibration results, an evaluation sequence with a different chessboard configuration (see Fig. 4 right) is used. The intrinsic camera parameters are fixed and only the poses are optimized. We compare the B-spline camera model with a generic single viewpoint radial symmetric camera model as described by Kannala et. al. in [7] with two tangential and three rotational distortion parameters.

The first lens is a low cost pinhole lens with 4mm focal length. We use two metrics to compare the two camera models. The first metric is the reprojection error. Usually in literature, only the mean reprojection error

$$e_{rm} = \frac{1}{N}\sum_{i=1}^{N} \|\mathbf{e}_{r,i}\| \tag{16}$$

is used, where $\mathbf{e}_{r,i}$ is from Eq. 7 and N are the number of detected chessboard corners. As the mean reprojection error only characterizes a small portion of the distribution, we are also using a smoothed two-dimensional histogram. On the x- and y-axis the reprojection errors in u and v are plotted and the height of the histogram is color-coded. For better visualization isolines are also plotted (see Fig. 5). As we made the assumption of a normal distributed chessboard corner detection, the histogram should also be a two-dimensional normal distribution. This is the case for both camera models and both lenses.

C. Windshield

As it is common for automated driving to place cameras behind windshields, we evaluated the influence of the windshield with respect to camera calibration. We use three cameras, two mounted on the roof and one behind the windshield. We have noticed that the effect of the windshield is not observable by using only a single camera, as the influence of the windshield can be compensated by a change in the chessboard poses. Two sequences with different angles are recorded and calibrated, where in the first one the camera was almost perpendicular to the windshield and in the second one

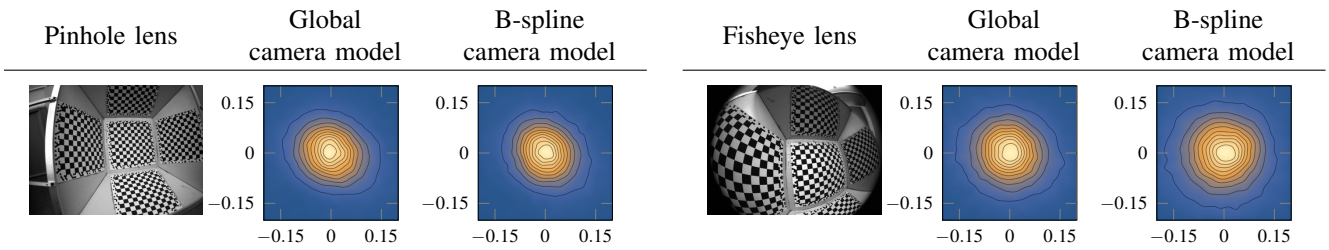

Fig. 5: Single camera calibration using a pinhole (left) and a fisheye (right) lens. The reprojection error is plotted as a smooth two-dimensional histogram for a global camera model ([7]) and the proposed B-spline camera model. The B-spline camera model can cope with both lens types and the reprojection errors are very similar (best viewed digitally with zoom).

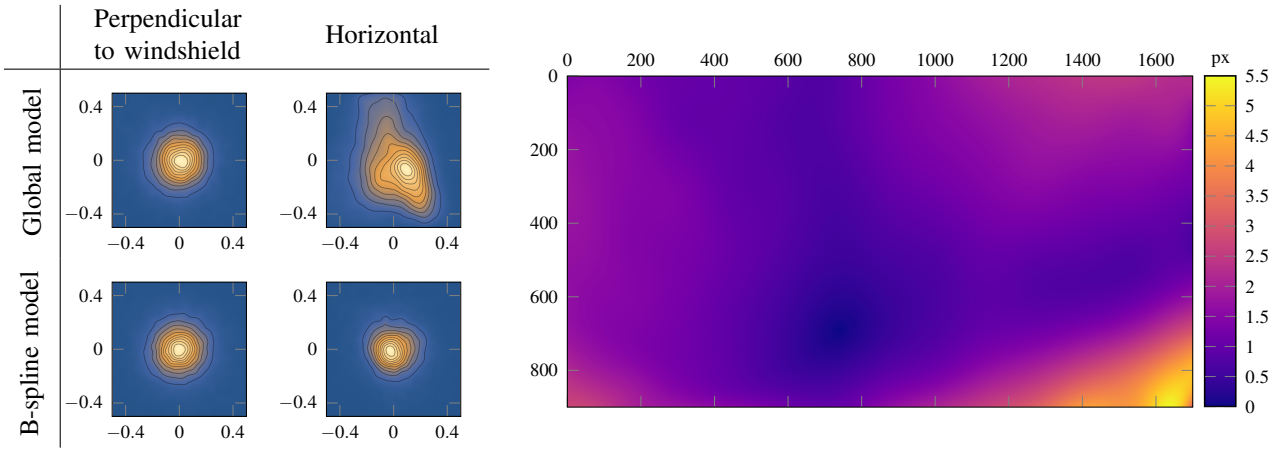

Fig. 6: Calibration result of a camera mounted behind a windshield. We use three cameras, two mounted on top of the vehicle and one behind the windshield. On the left side the reprojection error histogram for two different mounting positions of the camera behind the windshield is plotted. In the first one, the camera is oriented perpendicular to the windshield and in the second one the camera points forward (horizontal). In the right image, the difference of the pixel position of 3D points at infinity projected into the global and B-spline camera model is plotted (best viewed digitally with zoom).

the camera was mounted horizontally. The error histogram is shown in Fig. 6.

As one can clearly see, the mean reprojection error histogram for the global camera model increases a lot in the horizontally mounted case. Also a non-normal distribution is clearly visible. The B-spline camera model can cope with the distortions induced by the windshield.

To further analyze the influence of the windshield, we propose a measure between the difference of two camera models on a per pixel basis. This is achieved by first aligning the two camera models by minimizing the cord length at every pixel

$$\mathbf{R}^* = \arg\min_{\mathbf{R}} \sum_u \sum_v \left\| \mathcal{P}_{B,1}(u,v) - \mathbf{R}\,\mathcal{P}_{B,2}(u,v) \right\|, \qquad (17)$$

where $\mathbf{R}$ is the rotation matrix. With the aligned camera model, a 3D point at infinity is projected in image space and the difference of the two positions is used as a measure of how distinct the models in this area are. To efficiently implement this, we cast a ray at a certain pixel position (u,v) using one camera model and project a 3D point on that ray back in the image using the other camera model. This can be expressed as:

$$e_d(u,v) = \left\| \begin{pmatrix} u \\ v \end{pmatrix} - \mathcal{P}_{F,1}(\mathbf{R}^*\,\mathcal{P}_{B,2}(u,v)) \right\| \qquad (18)$$

The distance between those two positions is color-coded and shown in Fig. 6. Even though the difference of the mean reprojection error (see Tab. I) of the *windshield horizontal setup* is less than 0.3px, the difference between the two camera models are significant especially at the corners, where the difference is larger than five pixels.

D. Multi-camera calibration

In this setup six 5MP CMOS cameras are used (Flir BFS-PGE-50S5{C,M}-C), three behind the windshield facing forward, two to the side and one behind the rear window (see Fig. 7). This setup is challenging due to the small overlapping field of views, the various types of lenses and the mounting behind the windshield. As one can see, the mean reprojection error is smaller for every camera calibrated with the B-spline model. In case of the rear camera, the global camera model failed to converge due to the used wide angle lens mounted behind a windshield, which induces strong distortions at the edge of the image. The proposed B-spline camera model can handle such cases.

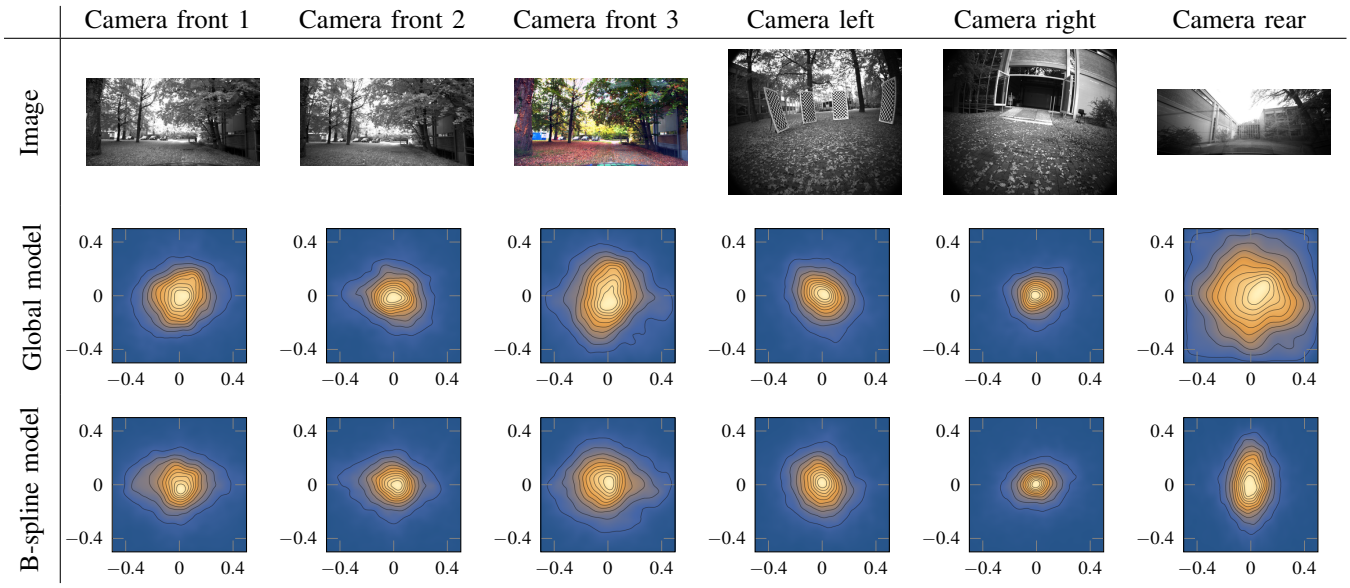

Fig. 7: Surround view camera calibration with six cameras. The top row shows the camera image, the second row the reprojection error histogram of a global camera model and the third row of the B-spline camera model. One can clearly see the benefit of using the B-spline camera model especially for the front color camera (camera front 3) and the rear camera (best viewed digitally with zoom).

V. CONCLUSION AND FUTURE RESEARCH

In this paper we proposed a local single viewpoint camera model based on B-splines. We showed how such a camera model can be integrated into an easy-to-use chessboard calibration framework by proposing a residual term specific to the proposed model. An extensive evaluation with single and multi-camera setups with up to six cameras and cameras mounted behind a windshield is used to demonstrate the benefits of the proposed camera model in comparison to global ones. We showed that the mean reprojection error is usually not sufficient for comparison, therefore we propose a two-dimensional reprojection error histogram. Further, we presented a way of how two camera models can be compared in a sense that differences are easily visible.

In the future, we will be working on how the number of measurements needed to calibrate the B-spline camera model can be reduced and will be estimating the uncertainty of the camera model.

REFERENCES

[1] M. D. Grossberg and S. K. Nayar, "A general imaging model and a method for finding its parameters," in *Computer Vision, 2001. ICCV 2001. Proceedings. Eighth IEEE International Conference on*, vol. 2. IEEE, 2001, pp. 108–115.

[2] S. Ramalingam and P. Sturm, "A unifying model for camera calibration," *IEEE transactions on pattern analysis and machine intelligence*, vol. 39, no. 7, pp. 1309–1319, 2017.

[3] P. Miraldo and H. Araujo, "Calibration of smooth camera models," *IEEE transactions on pattern analysis and machine intelligence*, vol. 35, no. 9, pp. 2091–2103, 2013.

[4] R. Tsai, "A versatile camera calibration technique for high-accuracy 3d machine vision metrology using off-the-shelf tv cameras and lenses," *IEEE Journal on Robotics and Automation*, vol. 3, no. 4, pp. 323–344, 1987.

[5] Z. Zhang, "A flexible new technique for camera calibration," *IEEE Transactions on pattern analysis and machine intelligence*, vol. 22, no. 11, pp. 1330–1334, 2000.

[6] D. Scaramuzza, A. Martinelli, and R. Siegwart, "A flexible technique for accurate omnidirectional camera calibration and structure from motion," in *Computer Vision Systems, 2006 ICVS'06. IEEE International Conference on*. IEEE, 2006, pp. 45–45.

[7] J. Kannala and S. S. Brandt, "A generic camera model and calibration method for conventional, wide-angle, and fish-eye lenses," *IEEE transactions on pattern analysis and machine intelligence*, vol. 28, no. 8, pp. 1335–1340, 2006.

[8] F. Bergamasco, L. Cosmo, A. Gasparetto, A. Albarelli, and A. Torsello, "Parameter-free lens distortion calibration of central cameras," in *Proceedings of the IEEE Conference on Computer Vision and Pattern Recognition*, 2017, pp. 3847–3855.

[9] D. Rosebrock and F. M. Wahl, "Generic camera calibration and modeling using spline surfaces," in *Intelligent Vehicles Symposium (IV), 2012 IEEE*. IEEE, 2012, pp. 51–56.

[10] D. Rosebrock, "The surface model - an uncertain continuous representation of the generic camera model and its calibration," Ph.D. dissertation, Feb 2016.

[11] W. V. D. Hodge, W. Hodge, and D. Pedoe, *Methods of algebraic geometry*. Cambridge University Press, 1994, vol. 2.

[12] A. K. Dunne, J. Mallon, and P. F. Whelan, "Efficient generic calibration method for general cameras with single centre of projection," *Computer Vision and Image Understanding*, vol. 114, no. 2, pp. 220–233, 2010.

[13] C. De Boor, *A practical guide to splines*, ser. Applied mathematical sciences. Berlin: Springer, 1978, vol. 27. [Online]. Available: https://cds.cern.ch/record/1428148

[14] T. Strauß, J. Ziegler, and J. Beck, "Calibrating multiple cameras with non-overlapping views using coded checkerboard targets," in *Intelligent Transportation Systems (ITSC), 2014 IEEE 17th International Conference on*. IEEE, 2014, pp. 2623–2628.

[15] T. Strauß, "Kalibrierung von multi-kamera-systemen-kombinierte schätzung von intrinsischem abbildungsverhalten der einzelnen kameras und deren relativer lage zueinander ohne erfordernis sich überlappender sichtbereiche," 2015.